ORIGINAL PAPER

Terahertz-infrared spectroscopy of *Shewanella oneidensis* MR-1 extracellular matrix

Z. V. Gagkaeva[1] · E. S. Zhukova[1] · V. Grinenko[2] ·
A. K. Grebenko[1] · K. V. Sidoruk[3] · T. A. Voeikova[3] ·
M. Dressel[1,4] · B. P. Gorshunov[1]

Abstract Employing optical spectroscopy we have performed a comparative study of the dielectric response of extracellular matrix and filaments of electrogenic bacteria *Shewanella oneidensis* MR-1, cytochrome c, and bovine serum albumin. Combining infrared transmission measurements on thin layers with data of the terahertz spectra, we obtain the dielectric permittivity and AC conductivity spectra of the materials in a broad frequency band from a few cm^{-1} up to 7000 cm^{-1} in the temperature range from 5 to 300 K. Strong absorption bands are observed in the three materials that cover the range from 10 to 300 cm^{-1} and mainly determine the terahertz absorption. When cooled down to liquid helium temperatures, the bands in *Shewanella oneidensis* MR-1 and cytochrome c reveal a distinct fine structure. In all three materials, we identify the presence of liquid bound water in the form of librational and translational absorption bands at $\approx$ 200 and $\approx$ 600 cm^{-1}, respectively. The sharp excitations seen above 1000 cm^{-1} are assigned to intramolecular vibrations.

✉ B. P. Gorshunov
bpgorshunov@gmail.com

[1] Moscow Institute of Physics and Technology, Dolgoprudny, Moscow Region, Russia

[2] Institute for Metallic Materials, IFW Dresden, Dresden, Germany

[3] Scientific Center of Russian Federation Research Institute for Genetics and Selection of Industrial Microorganisms, Moscow, Russia

[4] Physikalisches Institut, Universität Stuttgart, Stuttgart, Germany

1 Introduction

Charge transport is among the most important phenomena that ensure functioning of biological systems. Extracellular long-range charge transfer is of primary importance for the metabolism of various microbial forms of life. Extracellular filaments, which are the part of extracellular matrix of various electrogenic bacteria, were intensively studied during the last decade. Some of these bacteria are able to transfer electrons over amazingly long distances of dozens of micrometers [1–5]. A complete understanding of transport mechanisms in microbial filaments, as well as in biological objects in general, is presently lacking, and various viewpoints are under intense and lively debate. The mechanism of this transfer should be closely related to the structure and molecular dynamics of bacterial nanowires. For example, in the two most studied electrogenic species, *Shewanella oneidensis* and *Geobacter sulfurreducens*, the main conductive filaments are believed to have completely different structure and physiological origin; these are outer membrane appendages [6, 7] and tightly packed pilin protein (PilA), respectively, where pilin is considered to make the biggest contribution to the observed conductivity in *G. sulfurreducens* [4, 8–12]. All of these issues remain extremely challenging and are subject of intensive studies [2, 4, 8, 13–18]. From the viewpoint of experimental research, optical spectroscopy is among the most appropriate and direct methods for investigating these phenomena. Here, the term "optical spectroscopy" is used in a very broad sense and means investigation of electrodynamic properties of materials (absorption, refractive index, dielectric permittivity, AC conductivity, etc.) in a frequency range as wide as possible, from Hertz and sub-Hertz frequencies, radio and microwaves, via the typical optical range all the way up to X-rays. In the condensed matter physical community, these techniques have been used for many decades, providing unique information on temporal and spatial characteristics of various systems. With regard to biological objects, testing their reaction to the probing radiation with tunable frequency can deliver information on the objects properties in an extremely broad temporal and spatial range spanning from macroscopic scales where charge transport or movements of large molecular groups determine the response functions, down to $\approx 10^{-15}$ s and ≈ 1 nm, where the internal, localized vibrations of atoms composing bio-molecules reveal themselves. Electrical conductance in biological systems can be realized via electron/hole channels (hopping, tunneling, or probably, band–type mechanisms) or ionic transport through liquid bound water. Each process has its own specific frequency/temperature behavior [19], the study of which can allow the researcher to get insight into microscopic dynamics of charge carriers. The enormous sensitivity of optical spectra to the presence of water fractions in samples is another feature of the technique that can be utilized in the search for ionic conductivity. In our previous work [20], we have performed detailed spectroscopic investigations of charge transport mechanisms in lyophilized *S. oneidensis* MR-1 extracellular matrix and filaments (EMF). Radio-frequency ($\nu = 1$ Hz – 300 MHz) and terahertz ($\nu = 0.1$–1.6 THz) spectra of complex dielectric permittivity $\varepsilon^*(\nu,T) = \varepsilon'(\nu,T) + i\varepsilon''(\nu,T)$ and real part of AC conductivity $\sigma(\nu,T) = \nu\varepsilon''(\nu,T)/2$ of EMF and of two reference materials, cytochrome c (cytC) and bovine serum albumin (BSA), were measured at temperatures 10–300 K. Analysis of the radio-frequency response revealed in EMF clear signatures of free-carrier and hopping (presumably ionic) mechanisms of electrical charge transport. Here, we present the results of further studies of the dielectric and conduction properties of EMF of *Shewanella oneidensis* MR-1 obtained by performing first systematic

measurements of the *infrared* spectra of the complex dielectric permittivity and AC conductivity of EMF, CytC, and BSA at frequencies up to $\nu \approx 7000$ cm^{-1} and at temperatures from $T = 300$ K down to 5 K. The infrared spectra are analyzed together with our previous terahertz data [20]. In EMF and CytC, we detect clear signatures of hydration water that can provide a channel for the ionic transport before it freezes at around 250 K. In all three materials, we discover broad absorption bands covering the range from 10 to 300 cm^{-1}, that show fine structure at cryogenic temperatures in EMF and CytC.

2 Materials and methods

2.1 *Shewanella oneidensis* MR-1 strain origin

The strain *S. oneidensis* MR-1 was obtained by the Russian National Collection of Industrial Microorganisms, Scientific Center of Russian Federation - Research Institute for Genetics and Selection of Industrial Microorganisms (Moscow, Russia), from the collection of microorganisms of the Pasteur Institute (CIP106686, Paris France). The strain *S. oneidensis* MR-1 has number B9861 in the Russian National Collection of Industrial Microorganisms.

2.2 Cultivation of *Shewanella oneidensis* MR-1 strain

Initially, we used a standard cultivation method, which involves the use of a minimal medium with lactate. However, later we compared the different media, both standard and proprietary, including rich media TSB, etc. The comparison of the fuel cell operation using various media showed that the current obtained in the case of TSB medium and some other rich media is not less than the one obtained in case of minimal medium with lactate, while the duration of the stable fuel cell operation on a complete medium increases many times. The reproducibility and convergence of the results also increases during use of the complete media. Therefore, in the experiments designed to obtain a biomass grown under conditions of electron acceptor deficiency, we decided to utilize rich media. To generate conductive structures, *S. oneidensis* must be cultivated in in the absence of available final electron acceptors, which are certainly present in a rich medium. However, a stable current generation in MFC in case of rich medium indicates an excess of the potential electron donors and a deficiency of the acceptors. A simple experiment supports this fact. It is impossible to grow *S. oneidensis* in rich medium (as well as in a minimal medium with lactate) under anaerobic conditions since the availability of electron acceptors is diminished. However, the growth can be observed after addition of an excess electron acceptor like fumarate or Fe^{+3} or introduction of the anode into the medium. In the current study, the *S. oneidensis* MR-1 strain was grown on Petri dishes on agarized Luria–Bertani medium (LBM) during 48 h at 30 °C. For obtaining cell biomass, colonies from LBM were transferred into 100 ml of LB broth in a 750-ml flask and cultivated in aerobic conditions on a rotary shaker at 220 rpm at 30 °C for 18 h. Cells were sedimented by centrifugation at $6000 \times g$ for 20 min, washed with sterile deionized water of Milli-Q (Millipore, Burlington, MA, USA) under the same centrifugation conditions and resuspended in 2 ml of deionized water. The biomass was transferred into MM synthetic medium [21] with lactate concentration of 4 g/l and then introduced into the anode chamber of a microbial fuel cell.

2.3 Isolation of *Shewanella oneidensis* MR-1 bacterial extracellular matrix (EMF)

The bacterial fuel cells that produced electrical currents exceeding 30 μA were used for isolation of EMF. These current values agree well with the published data [21]. The procedure included the following steps. The cell culture grown on an anode was washed with 100 mM phosphate-buffer ed saline (pH 7.4) prepared from PBS tablets (Helicon, Moscow Russia) and pure water produced by Milli-Q integral water purification system (Merck Millipore, Burlington, MA, USA). After this, the cells were concentrated by means of centrifugation (30 min, Beckman Coulter Avanti J-26 centrifuge, rotor JLA 8.1, speed 5500 rpm). The precipitate was collected into 50-ml Falcon tubes. Every 5 ml of concentrated cells were diluted with 30 ml of Milli-Q water. The obtained suspension of cells was treated with intensive vortexing for avulsion of the filaments from the cells (maximal speed, Scientific Instruments Vortex-Genie 2, USA), for 10 min three times with two 5-min breaks in water with ice between vortexing. After this, 20 ml of Milli-Q water was added to each Falcon tube to make a quantity of 50 ml. The Falcon tubes were tightly shaken and then centrifuged for 15 min at $13000 \times g$ (Eppendorf 5810r centrifuge with FA-45-6-30 rotor). The supernatant was collected and treated with filtration through a 0.22-μm pore size Durapore membrane filter (Merck Millipore, Burlington, MA, USA). The precipitate was resuspended, vortexed for 5 min, and re-centrifuged according to the procedure described above. The second supernatant was also filtrated through a 0.22-μm Durapore membrane filter, mixed with the first supernatant, and then cooled down to –80 °C in plates with large surfaces for further lyophilization. A small volume of filtered supernatant was collected for atomic-force microscopy study of the sample.

The conductive filaments produced by *S. oneidensis* MR-1 are appendages of the bacterial outer membrane [6, 7]. The width of the appendages is much smaller than 0.22 μm, i.e., the size of the pore in the utilized filter. The membrane and appendages are supposed to contain multiheme cytochromes OmcA, MtrA, and MtrC, and the last cytochrome, being directly within the membrane, is surrounded by porin MtrB. The 'porin-cytochrome' model was also discussed in the article [22]. The appendages can be easily removed from the cells and isolated from the large cell debris impurities [2].

2.4 Lyophilization of EMF

The prepared and frozen extracellular matrix was lyophilized using a TFD 5503 freeze dryer (ilShin, South Korea). The lyophilization continued for 40 h with gradual temperature increase from –80 °C to 36 °C until the pressure of 0.010 mTorr was reached, yielding amorphous light-brown-colored powder.

2.5 The sources of reference proteins

Bovine serum albumin was supplied by Amresco, (Radnor, PA, USA) (code 0332). Bovine heart cytochrome c was supplied by Sigma-Aldrich, (St.Louis, MO, USA) (code C3131).

2.6 Sample pellet preparation

Amorphous powders of BSA, CytC, and EMF were pressed into pellets using a mold with a diameter of 10 mm. The pellets of BSA and CytC were obtained under a pressure of 10 atm. The pellets of EMF were obtained under a pressure of 5 atm.

2.7 Preparation of thin-layer samples

Amorphous powders of BSA and CytC were dissolved in deionized water (Millipore Milli-Q) to form saturated solutions. These solutions were drop-casted on a polyethylene film (10-μm thickness) and incubated at RH 20% and room temperature for 3 days. Finally, thin (about 0.1 mm) samples on polyethylene film were obtained that were used for the measurements of transmission coefficients at terahertz and infrared frequencies.

2.8 Confirmation of the presence of filaments in EMF by means of atomic-force microscopy

To confirm the presence of filaments in solutions that were used for preparation of EMF samples, we utilized drop-cast deposition on silicon wafers with subsequent study of the wafer surface by means of atomic-force microscopy technique. Scans were done in tapping mode on NTM-DT Smena Atomic Force Microscope system. Regular silicon cantilevers with resonant frequency of 350 kHz were used. An example of the scan is presented in Fig. 6.

3 Experimental results and discussion

Since the pure fraction of the filaments is not the only component utilized by these bacteria for extracellular charge conduction, our purpose was to investigate the *integral* dielectric/conducting properties of the outer cell matrix including filaments and other components synthesized under anaerobic conditions. The results on EMF were compared with the data on two reference commercially available materials, cytochrome c and bovine serum albumin.

Infrared (IR) measurements at frequencies up to 7000 cm^{-1} were performed in the transmission mode using Fourier-transform spectrometer Vertex 80v. Transmission coefficient spectra were measured on the EMF, CytC, and BSA samples prepared in the form of layers about 0.1 mm thick made on thin (10 μm) polyethylene films as transparent supports (details given in the Materials and methods section). The same samples were measured in the terahertz (THz) range using a coherent-source spectrometer based on backward-wave oscillators [23] and pulsed time-domain TeraView spectrometer. At THz frequencies, transmissivities of thick (≈ 1 mm) pellets used in our previous study [20] were also measured. The temperature-dependent experiments were performed in home-made optical cryostats.

Transmissivities of thick pellets and film samples on polyethylene substrates were processed using well-known [19, 24] expressions for transmission coefficients of single or double-layered systems, respectively. Examples of such processing of the spectra are shown by lines in Figs. 1a, 2a, and 3a. Here, low-frequency oscillations in the transmission coefficient spectra are due to multiple reflections of the radiation within the plane-parallel samples (Fabry–Perot effect); these interferometric fringes are not so well pronounced in the spectra of thin samples. At higher frequencies, deep minima in the transmissivity spectra (note logarithmic scale along the vertical axes) are caused by absorption lines and were fitted with the Lorentzians

$$\varepsilon^*(\nu) = \varepsilon^{'}(\nu) + i\varepsilon^{''}(\nu) = \frac{f}{\left(\nu_0^2 - \nu^2\right) + i\nu_0\gamma},$$ (1)
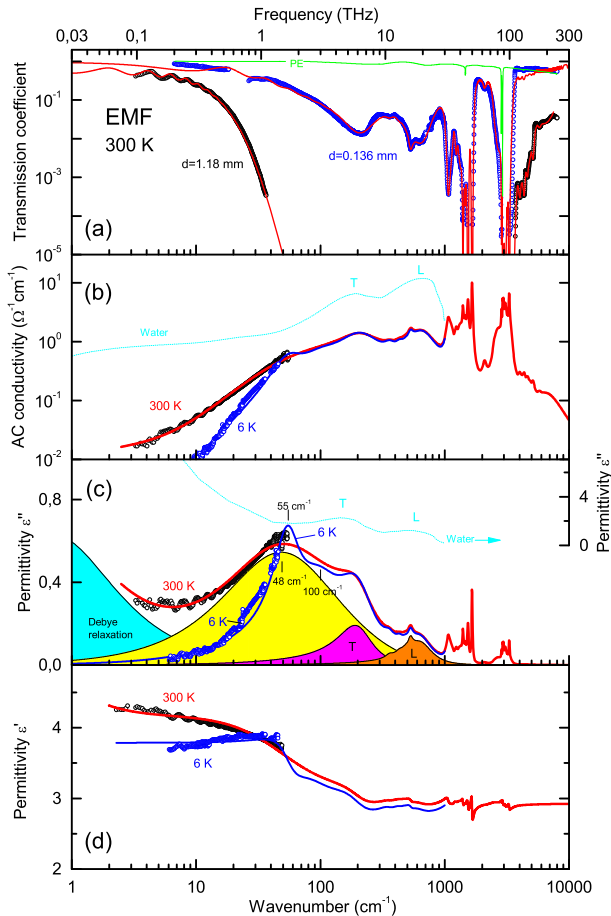
Fig. 1 a Room-temperature terahertz-infrared spectra of the transmission coefficient of plane-parallel EMF samples 1.18 mm thick (pellet used in experiments in [20]) and 0.136 mm thick (layer prepared on polyethylene film 10 μm thick, as described in the Materials and methods section). *Dots* are measured data and the *lines* correspond to least-square fits, as described in the text. The transmissivity of the polyethylene (PE) film is shown separately. **b**, **c**, **d** Spectra of AC conductivity (**b**) and imaginary (**c**) and real (**d**) parts of dielectric permittivity of EMF measured at two temperatures as indicated. *Open dots* correspond to the data from [20] that was directly obtained using THz spectrometers. *Lines* correspond to the least-square fits as described in the text. On panel (**c**), for room temperature, separately shown are components corresponding to the lowest-frequency contribution described with the Debye relaxational term (*blue*), to the bands located at ≈ 200 cm^{-1} (*magenta*) and ≈ 600 cm^{-1} (*brown*) associated with translational (T) and librational (L) vibrations of bound water molecules, respectively, and to the broad THz band (*yellow*). *Dotted lines* (*cyan*) show the spectra of AC conductivity (**b**) and imaginary dielectric permittivity (**c**) spectra of liquid water taken from [25–27]

where $f = \Delta\varepsilon\nu_0^2$ is the oscillator strength of the resonance, $\Delta\varepsilon$ is its dielectric contribution, ν_0 represents the resonance frequency and γ is the damping factor. Broad-band THz-IR spectra of real and imaginary parts of the permittivity and AC conductivity were obtained by merging the directly measured corresponding THz values from [20] (dots in Figs. 1, 2, and 3) with the spectra, derived by least-square fits of the IR transmission coefficients. We associate the rich sets of absorption features above ≈ 1000 cm^{-1} with intramolecular modes and vibrations of molecular groups, as discussed for BSA in [28, 29] and for CytC in [30–32]. Tables 1, 2, and 3 summarize parameters of absorption
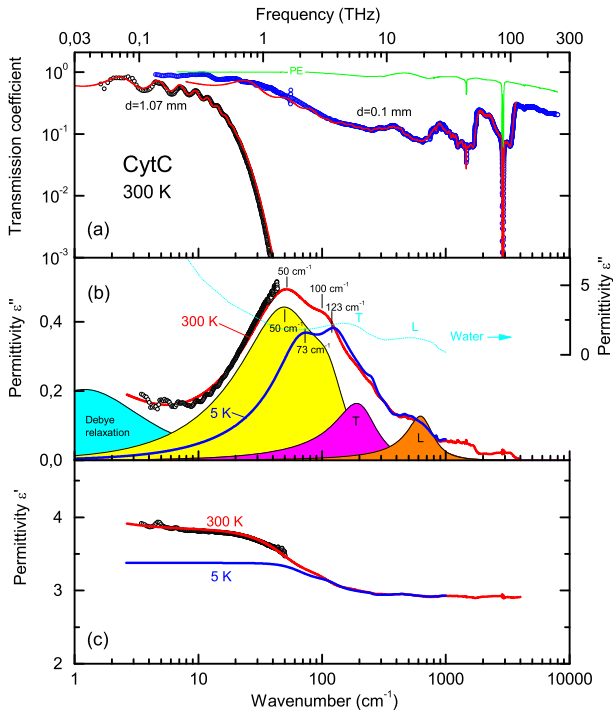
Fig. 2 **a** Room-temperature terahertz-infrared spectra of transmission coefficient of plane-parallel CytC samples 1.07 mm thick (pellet used in experiments in [20]) and 0.1 mm thick (layer on polyethylene film 10 μm thick, as described in the Materials and methods section). *Dots* are measured data and the *lines* correspond to least-square fits, as described in the text. Transmissivity of the polyethylene (PE) film is shown separately. **b, c** Spectra of imaginary (**b**) and real (**c**) parts of dielectric permittivity of CytC measured at two temperatures as indicated. *Open dots* show the data from [20] directly obtained using THz spectrometers. *Lines* correspond to the results of least-square fits. In **b**, for room temperature, separately shown are components corresponding to the lowest-frequency contribution described with the Debye relaxational term (*blue*), to the bands located at ≈ 200 cm^{-1} (*magenta*) and ≈ 600 cm^{-1} (*brown*) associated with translational (T) and librational (L) vibrations of bound water molecules, respectively, and to the broad THz band (*yellow*). *Dotted line* (*cyan*) shows imaginary dielectric permittivity spectrum of liquid water taken from [25–27]

resonances determined by least-square processing of the transmission coefficient spectra with expression (1). Below we focus on lower-energy excitations that are expected to involve long-range movements of large assemblies of molecules and molecular subunits.

3.1 Spectral signatures of bound water

At room temperature, a clear upturn towards low frequencies is detected (see also [20]) below ≈ 10 cm^{-1} in the spectra of real and imaginary permittivities of EMF and CytC (see Figs. 1b, c and 2b, c, respectively). This is a typical signature of relaxational-type dispersion and it was modeled [20] by the Debye relaxational expression $\varepsilon^*_D = \Delta\varepsilon/[1 + i\omega\tau]$, where $\Delta\varepsilon$ is the relaxation strength, τ is the relaxation time, and ω is the circular frequency [33]. (Since our measured THz spectra contain only the higher-frequency part of the relaxation, we were not able to extract precise numerical values of $\Delta\varepsilon$ and τ). Such behavior resembles the dispersion observed in the microwave dielectric response of bulk liquid water (see, e.g., [34]); as an example, the spectra of the imaginary permittivity and AC conductivity of water are presented
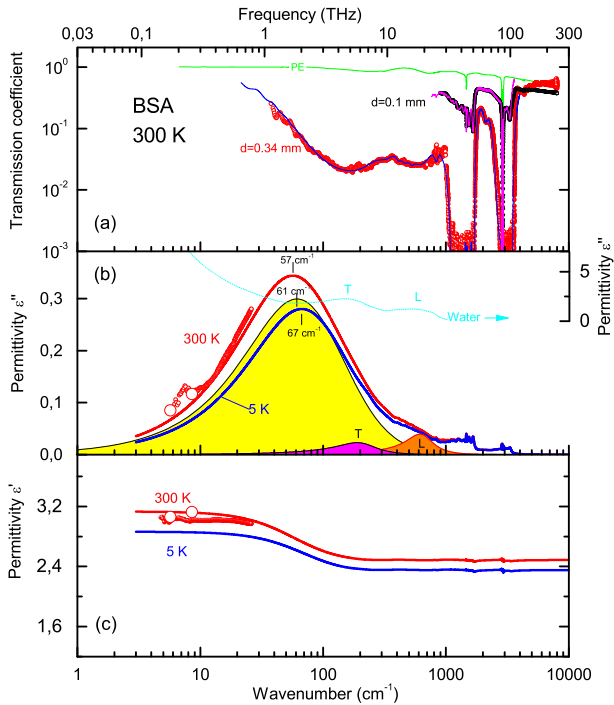
Fig. 3 **a** Room-temperature terahertz-infrared spectra of transmission coefficient of plane-parallel BSA samples 1.07 mm thick (pellet used in experiments in [20]) and 0.1 mm thick (layer on polyethylene film 10 μm thick, as described in the Materials and methods section). *Dots* are measured data and the *lines* correspond to least-square fits, as described in the text. Transmissivity of the polyethylene (PE) film is shown separately. **b**, **c** Spectra of imaginary (**b**) and real (**c**) parts of dielectric permittivity of BSA measured at two temperatures as indicated. *Open dots* show the data directly obtained in [20] using THz spectrometers. *Lines* correspond to the results of least-square fits described in the text. In **b**, for room temperature, separately shown are components corresponding to the bands located at ≈ 200 cm^{-1} (*magenta*) and ≈ 600 cm^{-1} (*brown*) associated with translational (T) and librational (L) vibrations of bound water molecules, respectively, and to the broad THz band (*yellow*). The *dotted line* (*cyan*) shows imaginary dielectric permittivity spectrum of liquid water taken from [25–27]

by dotted lines in Figs. 1b, c and 2b. According to [20], we believe that the observed lowest-frequency relaxation in the spectra of EMF and CytC is connected with the bound hydration water present in these two samples; its significantly smaller strength $\Delta\varepsilon$, compared to bulk water, is due to lower water content in the samples. (Similar Debye-type relaxation due to bound water was seen in a number of other biological objects, see, e.g., [35–38]). Our assumption is confirmed by the temperature evolution of the relaxation spectra: the Debye-like features disappear when the EMF and CytC samples are cooled down (Figs. 1 and 2), which we connect with the freezing of bound water fraction. Figure 4 shows the temperature dependences of the imaginary permittivity measured at a fixed frequency of 10 cm^{-1}. The value of $\varepsilon''(10$ cm$^{-1})$ in EMF strongly decreases below 300 K and gets nearly temperature independent below 230–250 K; the decrease happens exactly in the temperature interval where a knee-like anomaly is observed of the specific heat of EMF (Fig. 3B in [20]), that is typical for freezing of "biological water". CytC and BSA reveal significantly weaker changes of absorption $\varepsilon''(10$ cm$^{-1})$ at these temperatures. Spectral signatures of bound water in EMF, CytC, and BSA are observed also at infrared frequencies. Here, two pronounced bands show up around 200 and 600 cm^{-1}, where translational and librational vibrations of H_2O molecules,

Table 1 Parameters of Lorentzians (Eq. 1) used to describe the absorption resonances observed in the room-temperature infrared transmission coefficient spectrum of extracellular matrix of electrogenic bacteria *S. oneidensis* MR-1

Resonance number	Frequency ν_0 (cm^{-1})	Damping γ (cm^{-1})	Dielectric contribution $\Delta\varepsilon$, $\cdot 10^{-5}$	Oscillator strength f (cm^{-2})	Oscillator strength f (intensity), log scale
1	1070	90	910	10425	
2	1130	65	200	2506	
3	1160	30	30	390	
4	1240	80	310	4780	
5	1310	70	196	3360	
6	1350	57	129	2340	
7	1400	44	417	8190	
8	1460	55	240	5165	
9	1540	50	583	13770	
10	1660	34	724	19990	
11	2095	170	50	2250	
12	2515	167	68	4300	
13	2625	174	57	3945	
14	2740	356	327	24620	
15	2860	35	48	3920	
16	2875	15	10	827	
17	2930	22	56	4764	
18	2960	39	83	7277	
19	3075	168	413	39000	
20	3200	50	27	2740	
21	3300	65	198	21535	
22	3410	197	100	11655	
23	3955	150	2	270	
24	4045	220	7	1180	
25	4186	155	2	305	
26	4355	225	9	1615	
27	4630	340	10	2160	
28	4855	229	2	515	
29	5130	326	6	1644	
30	6610	4060	60	26330	

ν_0 – resonance frequency, γ - damping, $\Delta\varepsilon$ – dielectric contribution, $f = \Delta\varepsilon\nu_0^2$ – oscillator strength (intensity). The result of the least-square processing of the spectrum is presented by a *solid line* in Fig. 1a. For convenience, intensities of the resonances are indicated in the left column by *bars* in a log scale

respectively, are present in the spectra of bulk liquid water; they are marked with "T" and "L" in Figs. 1b, c and 2b. By analogy with liquid water, we associate the bands observed in all three samples at ≈200 and ≈600 cm^{-1} with translational (T) and librational (L) vibrations of bound water molecules. Signs of these T- and L-bands are present in the spectra also at lower temperatures (down to 5 K), which is consistent with their presence in water ice [39].

In [20], we have estimated the water content in the samples by thermogravimetry technique. The analysis revealed that the BSA and the CytC samples contained a noticeably larger

Table 2 Parameters of Lorentzians (Eq. 1) used to describe the absorption resonances observed in the room-temperature infrared transmission coefficient spectrum of cytochrome c

Resonance number	Frequency ν_0 (cm^{-1})	Damping γ (cm^{-1})	Dielectric contribution $\Delta\varepsilon$, $\cdot 10^{-5}$	Oscillator strength f(cm^{-2})	Oscillator strength f (intensity), log scale
1	1030	100	152	1620	
2	1105	74	132	1608	
3	1169	73	106	1445	
4	1244	84	166	2570	
5	1308	95	113	1940	
6	1390	114	169	3262	
7	1463	14	18	381	
8	1520	223	385	8908	
9	1672	190	259	7254	
10	2094	543	275	12065	
11	2482	399	105	6464	
12	2742	539	263	19781	
13	2858	12	20	1636	
14	2927	22	38	3275	
15	2963	39	3	233	
16	3063	250	60	5650	
17	3200	102	4	424	
18	3345	459	218	24417	

ν_0 – resonance frequency, γ - damping, $\Delta\varepsilon$ – dielectric contribution, $f = \Delta\varepsilon\nu_0^2$ – oscillator strength (intensity). The result of the least-square processing of the spectrum is presented by *solid line* in Fig. 2a. For convenience, intensities of the resonances are indicated in the left column by *bars* in a log scale

amount of water relative to EMF[1]. At the same time, the water-related Debye-like relaxation is most strongly pronounced in EMF; it is about two times weaker in CytC and not seen at all in BSA. Also, the strong anomalies seen in specific heat in [20] and dielectric absorption of EMF are absent in CytC and BSA (Figs. 1, 2, and 3). The same tendency applies to the T- and L-bands: being comparable in intensity in EMF and CytC, they are hardly distinguished in the IR spectra of BSA (Fig. 3b). These observations indicate that liquid water should be much stronger bound in BSA and CytC than in EMF. Strong coupling of water molecules to the surrounding is also demonstrated by Fig. 5, where the absorption spectra of the studied samples are displayed in the frequency range where the H_2O intramolecular modes ν_1 (symmetric stretch), ν_2 (bending), and ν_3 (asymmetric stretch) could be observed; for a free H_2O molecule, these modes are located at $\nu_1 = 3656.65$ cm^{-1}, $\nu_2 = 1594.59$ cm^{-1}, and $\nu_3 = 3755.79$ cm^{-1} [40]. Though certain structures are seen in the vicinity of the ν_2 mode (again, more intensive in EMF), no absorption peaks are visible close enough to ν_1 and ν_3. The shifts

---

[1] The formal amount of water in EMF is higher that the one in CytC and BSA. However, the water in our samples is in three different states: bulk, loosely bound and bound. We assume, that phenomena described here are related to the behavior of loosely bound water, the amount of which is lower in EMF. For more details, see [20]

Table 3 Parameters of Lorentzians (Eq. 1) used to describe the absorption resonances observed in the room-temperature infrared transmission coefficient spectrum of bovine serum albumin

Resonance number	Frequency ν_0 (cm^{-1})	Damping γ (cm^{-1})	Dielectric contribution $\Delta\varepsilon$, $\cdot 10^{-5}$	Oscillator strength f(cm^{-2})	Oscillator strength f (intensity), log scale
1	1030	65	30	314	
2	1105	104	300	365	
3	1170	60	75	1020	
4	1255	117	246	3860	
5	1310	116	116	1987	
6	1400	109	206	4022	
7	1460	14	18	380	
8	1540	93	250	5934	
9	1660	80	136	3744	
10	209	250	37	1643	
11	2480	440	20	1212	
12	2740	540	270	20327	
13	2860	12	28	2297	
14	2915	11	47	3970	
15	2960	39	4	375	
16	3060	250	86	8070	
17	3200	100	12	1261	
18	3410	265	142	16516	
19	4330	110	2	333	
20	5785	1290	11	3772	

ν_0 – resonance frequency, γ - damping, $\Delta\varepsilon$ – dielectric contribution, $f = \Delta\varepsilon\nu_0^2$ – oscillator strength (intensity). The result of the least-square processing of the spectrum is presented by *solid line* in Fig. 3a. For convenience, intensities of the resonances are indicated in the left column by *bars* in a log scale

in the mode positions from their free-molecular locations in EMF, CytC, and BSA are attributed to considerable coupling of the H_2O molecules to the molecular environment and corresponding renormalization of intramolecular bonds strength [41–44].
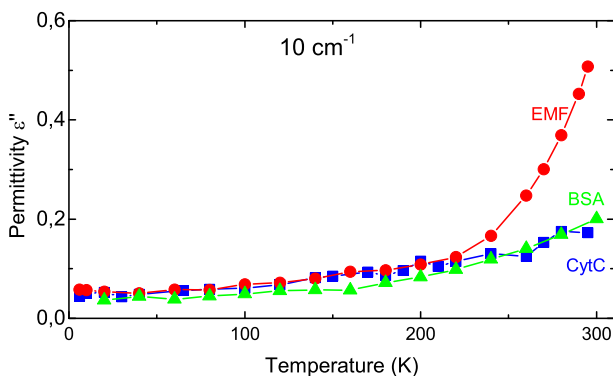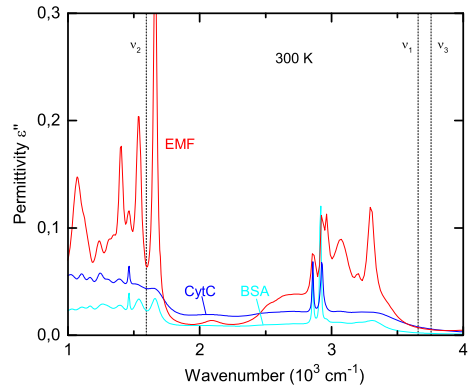

Fig. 4 Temperature dependence of imaginary part of dielectric permittivity of EMF, CytC, and BSA at a frequency 10 cm^{-1}

3.2 Terahertz absorption bands

As can be seen from Fig. 1c, the terahertz-infrared electrodynamic response in EMF is dominated by a broad band that spans from ≈ 10 to ≈ 300 cm^{-1}. Similar bands are also observed in CytC and BSA (Figs. 2 and 3). Earlier terahertz measurements on CytC [45–48], BSA [49, 50], and other biological systems [49, 51–54] reveal a continuously increasing featureless absorption that is usually ascribed to a glassy background due to a Debye-like quadratic growth of the vibrational density of states (VDOS) of numerous vibrations of protein molecules and water-protein complexes [49, 54–59]. Basing on our data that cover not just THz but also higher-frequency infrared range, we conclude that the terahertz absorption in EMF, CytC, and BSA is essentially nothing but the low-frequency slope of the bands centered around 48 cm^{-1} in EMF (Fig. 1), 50 cm^{-1} in CytC (Fig. 2), and 61 cm^{-1} in BSA (Fig. 3) with additional contribution coming at high temperatures from hydration water-related relaxation, though certain admixture from VDOS cannot be excluded. The monotonous
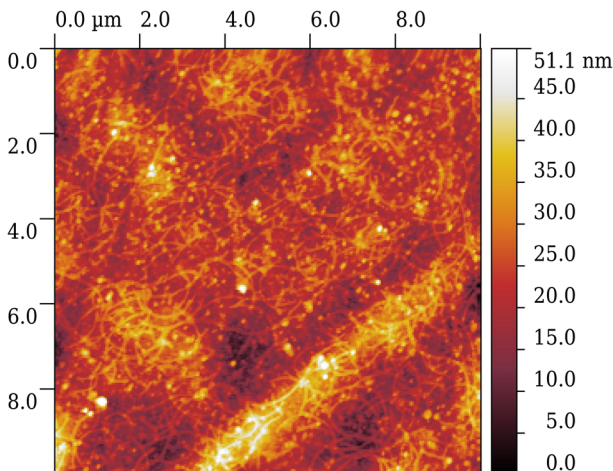

Fig. 6 Atomic-force microscopy image of the filaments in the suspension utilized for preparation of EMF samples

decrease with growing frequency (10–100 cm^{-1}) of the room-temperature real permittivities ε' (Figs. 1d, 2c, and 3c) indicates the strongly damped character of the THz bands. Corresponding numerical estimates of the damping factors γ/ν_0 (see Eq. 1) give the values of ≈ 3, ≈ 2.3, and ≈ 2.6 for EMF, CytC, and BSA, respectively. During cooling, the hydration water in EMF and CytC freezes out (in [20], see also Fig. 4) leading to certain narrowing of the THz bands. At liquid helium temperatures, two components of the bands are clearly resolved with central frequencies 55 cm^{-1} and 100 cm^{-1} in EMF and 73 cm^{-1} and 123 cm^{-1} in CytC (blue lines in Figs. 1 and 2). Note that the two-component structure of the band in CytC is resolved already at room temperature, albeit at significantly lower frequencies, 52 cm^{-1} and 100 cm^{-1}. Similar multi-component bands were observed in the terahertz absorption spectra of lysozyme [35] and in Raman spectra of lysozyme and DNA [36], with the frequency positions of the modes (Table 1 in [35] and Tables 1, 2 in [36]) very close to those obtained in the present work. This means that the materials studied here and in [35, 36] have similar molecules and/or molecular complexes. The effect of cooling is much less pronounced in the THz spectra of BSA where the THz band slightly decreases in amplitude with no noticeable change in damping.

We believe that the pronounced decrease of the THz absorptivity in EMF taking place between 230 and 300 K must be ascribed mainly to freezing of the bound water and cannot be explained by the dynamic transition, that is, by the change in flexibility of organic molecules in protein systems, characterized by a rapid increase in the mean square atomic displacements at 180–220 K in hydrated proteins [60, 61]. The reason is the strong water-freezing anomaly in the specific heat of EMF [20] that is not supposed to accompany the dynamic transition [54]. It is worth noting that the temperature changes in the THz dielectric response of lysozyme measured in Ref. [8] were not interpreted by the dynamical transition concept, but ascribed to a blue shift of water–protein relaxation. On the other hand, the absence of pronounced specific heat anomaly in CytC and BSA [20] indicates that effects related to the dynamical transition could play a certain role in determining the temperature variation of the THz absorption in these two materials [46, 62].

4 Conclusions

From our infrared spectroscopy, we obtained the transmission coefficient of thin (≈ 0.1 mm) layers of extracellular matrix of electrogenic bacteria *S. oneidensis* MR-1 (EMF), cytochrome c (CytC) and bovine serum albumin (BSA); the spectra cover the frequency range up to 7000 cm^{-1} and temperatures from 5 to 300 K. The transmissivity results are supplemented by previously obtained terahertz data in order to obtain the broad-band spectra of the real and imaginary parts of dielectric permittivity and real part of AC conductivity of the three materials. At lowest terahertz frequencies (below ≈ 10 cm^{-1}), we detect a pronounced dielectric relaxation in the spectra of EMF and CytC and ascribe it to the response of hydration water that can provide a channel for ionic transport. In all three materials, broad infrared absorption bands of yet unknown origin are discovered; we demonstrate that the bands are mainly responsible for absorption of electromagnetic radiation observed in previous terahertz experiments. Rich sets of intramolecular absorption lines is detected at frequencies above 1000 cm^{-1} and their parameters are determined.

Author contributions T.A.V. and B.P.G. designed the research; K.V.S. and T.A.V. performed cultivation of *Shewanella oneidensis* MR-1, A.K.G. prepared EMF, Z.V.G., E.S.Z, V.G., K.V.S. and A.K.G. performed research; Z.V.G., E.S.Z. and V.G. analyzed data; B.P.G and M.D. wrote the paper.

Compliance with ethical standards

Competing interests The authors declare that they have no competing financial interests.

References

1. Veazey, J.P., Reguera, G., Tessmer, S.H.: Electronic properties of conductive pili of the metal-reducing bacterium *Geobacter sulfurreducens* probed by scanning tunneling microscopy. Phys. Rev. E **84**, 1–4 (2011). https://doi.org/10.1103/PhysRevE.84.060901
2. Leung, K.M., Wanger, G., El-Naggar, M.Y., Gorby, Y., Southam, G., Lau, W.M., Yang, J.: *Shewanella oneidensis* MR-1 bacterial nanowires exhibit p-type, tunable electronic behavior. Nano Lett. **13**, 2407–2411 (2013). https://doi.org/10.1021/nl400237p
3. El-Naggar, M.Y., Wanger, G., Leung, K.M., Yuzvinsky, T.D., Southam, G., Yang, J., Lau, W.M., Nealson, K.H., Gorby, Y.A.: Electrical transport along bacterial nanowires from *Shewanella oneidensis* MR-1. Proc. Natl. Acad. Sci. U. S. A. **107**, 18127–18131 (2010). https://doi.org/10.1073/pnas.1004880107
4. Malvankar, N.S., Vargas, M., Nevin, K.P., Franks, A.E., Leang, C., Kim, B.-C., Inoue, K., Mester, T., Covalla, S.F., Johnson, J.P., Rotello, V.M., Tuominen, M.T., Lovley, D.R.: Tunable metallic-like conductivity in microbial nanowire networks. Nat. Nanotechnol. **6**, 573–579 (2011). https://doi.org/10.1038/nnano.2011.119
5. Malvankar, N.S., Yalcin, S.E., Tuominen, M.T., Lovley, D.R.: Visualization of charge propagation along individual pili proteins using ambient electrostatic force microscopy. Nat. Nanotechnol. **9**, 1012–1017 (2014). https://doi.org/10.1038/nnano.2014.236
6. Pirbadian, S., Barchinger, S.E., Leung, K.M., Byun, H.S., Jangir, Y., Bouhenni, R.A., Reed, S.B., Romine, M.F., Saffarini, D.A., Shi, L., Gorby, Y.A., Golbeck, J.H., El-Naggar, M.Y.: *Shewanella oneidensis* MR-1 nanowires are outer membrane and periplasmic extensions of the extracellular electron transport components. Proc. Natl. Acad. Sci. U. S. A. **111**, 12883–12888 (2014). https://doi.org/10.1073/pnas.1410551111
7. Subramanian, P., Pirbadian, S., El-Naggar, M.Y., Jensen, G.J.: The ultrastructure of *Shewanella oneidensis* MR-1 nanowires revealed by electron cryo-tomography. bioRxiv. (2017)
8. Malvankar, N.S., Vargas, M., Nevin, K., Tremblay, P., Evans-Lutterodt, K., Nykypanchuk, D.: Structural basis for metallic-like conductivity in microbial nanowires. mBio **6**(2), e00084 (2015). https://doi.org/10.1128/mBio.00084-15
9. Xiao, K., Malvankar, N.S., Shu, C., Martz, E., Lovley, D.R., Sun, X.: Low-energy atomic models suggesting a pilus structure that could account for electrical conductivity of *Geobacter sulfurreducens* pili. Sci. Rep. **6**, 23385 (2016). https://doi.org/10.1038/srep23385
10. Malvankar, N.S., Lovley, D.R.: Microbial nanowires: a new paradigm for biological electron transfer and bioelectronics. ChemSusChem **5**, 1039–1046 (2012). https://doi.org/10.1002/cssc.201100733
11. Adhikari, R.Y., Malvankar, N.S., Tuominen, M.T., Lovley, D.R.: Conductivity of individual *Geobacter* pili. RSC Adv. **6**, 8354–8357 (2016). https://doi.org/10.1039/C5RA28092C
12. Vargas, M., Malvankar, N.S., Tremblay, P.-L., Leang, C., Smith, J.A., Patel, P., Snoeyenbos-West, O., Synoeyenbos-West, O., Nevin, K.P., Lovley, D.R.: Aromatic amino acids required for pili conductivity and long-range extracellular electron transport in *Geobacter sulfurreducens*. mBio **4**, e00105 (2013). https://doi.org/10.1128/mBio.00105-13
13. Smith, D.M.A., Rosso, K.M.: Possible dynamically gated conductance along heme wires in bacterial multiheme cytochromes. J. Phys. Chem. B **118**, 8505–8512 (2014). https://doi.org/10.1021/jp502803y
14. El-Naggar, M.Y., Gorby, Y.A., Xia, W., Nealson, K.H.: The molecular density of states in bacterial nanowires. Biophys. J. **95**, L10–L12 (2008). https://doi.org/10.1529/biophysj.108.134411

15. Breuer, M., Rosso, K.M., Blumberger, J., Butt, J.N.: Multi-haem cytochromes in *Shewanella oneidensis* MR-1: structures, functions and opportunities. J. R. Soc. Interface **12**, 20141117 (2015). https://doi.org/10.1098/rsif.2014.1117

16. Yan, H., Chuang, C., Zhugayevych, A., Tretiak, S., Dahlquist, F.W., Bazan, G.C.: Inter-aromatic distances in *Geobacter sulfurreducens* pili relevant to biofilm charge transport. Adv. Mater. **27**, 1908–1911 (2015). https://doi.org/10.1002/adma.201404167

17. Grebenko, A., Dremov, V., Barzilovich, P., Bubis, A., Sidoruk, K., Voeikova, T., Gagkaeva, Z., Chernov, T., Korostylev, E., Gorshunov, B., Motovilov, K.: Impedance spectroscopy of single bacterial nanofilament reveals water-mediated charge transfer. PLoS ONE **13**, 1–17 (2018). https://doi.org/10.1371/journal.pone.0191289

18. Zaytsev, K.I., Kudrin, K.G., Karasik, V.E., Reshetov, I. V., Yurchenko, S.O.: In vivo terahertz spectroscopy of pigmentary skin nevi: pilot study of non-invasive early diagnosis of dysplasia. Appl. Phys. Lett. **106**, (2015). https://doi.org/10.1063/1.4907350

19. Dressel, M., Gruner, G.: Electrodynamics of Solids. Cambridge University Press, Cambridge (2002)

20. Motovilov, K.A., Savinov, M., Zhukova, E.S., Pronin, A.A., Gagkaeva, Z. V., Grinenko, V., Sidoruk, K. V., Voeikova, T.A., Barzilovich, P.Y., Grebenko, A.K., Lisovskii, S. V., Torgashev, V.I., Bednyakov, P., Pokorný, J., Dressel, M., Gorshunov, B.P.: Observation of dielectric universalities in albumin, cytochrome c and *Shewanella oneidensis* MR-1 extracellular matrix. Sci. Rep. **7**, 15731 (2017). https://doi.org/10.1038/s41598-017-15693-y

21. Logan, B.E., Hamelers, B., Rozendal, R., Schröder, U., Keller, J., Freguia, S., Aelterman, P., Verstraete, W., Rabaey, K.: Microbial fuel cells: methodology and technology. Environ. Sci. Technol. **40**, 5181–5192 (2006)

22. Richardson, D.J., Butt, J.N., Fredrickson, J.K., Zachara, J.M., Shi, L., Edwards, M.J., White, G., Baiden, N., Gates, A.J., Marritt, S.J., Clarke, T.A.: The "porin-cytochrome" model for microbe-to-mineral electron transfer. Mol. Microbiol. **85**, 201–212 (2012). https://doi.org/10.1111/j.1365-2958.2012.08088.x

23. Gorshunov, B., Volkov, A., Spektor, I., Prokhorov, A., Mukhin, A., Dressel, M., Uchida, S., Loidl, A.: Terahertz BWO-spectrosopy. Int. J. Infrared Millimeter Waves **26**, 1217–1240 (2005). https://doi.org/10.1007/s10762-005-7600-y

24. Born, M., Wolf, E.: Principles of Optics. Pergamon, Oxford (1980)

25. Downing, H.D., Williams, D.: Optical constants of water in the infrared. J. Geophys. Res. **80**, 1656–1661 (1975). https://doi.org/10.1029/JC080i012p01656

26. Zelsmann, H.R.: Temperature dependence of the optical constants for liquid H_2O and D_2O in the far IR region. J. Mol. Struct. **350**, 95–114 (1995). https://doi.org/10.1016/0022-2860(94)08471-S

27. Liebe, H.J., Hufford, G.A., Manabe, T.: A model for the complex permittivity of water at frequencies below 1 THz. Int. J. Infrared Millimeter Waves **12**, 659–675 (1991). https://doi.org/10.1007/BF01008897

28. Grdadolnik, J., Marechal, Y.: Bovine serum albumin observed by infrared spectrometry. II. Hydration mechanisms and interaction configurations of embedded H_2O molecules. Biopolymers **62**, 54–67 (2001). https://doi.org/10.1002/1097-0282(2001)62:1<54::AID-BIP70>3.0.CO;2-4

29. Grdadolnik, J., Marechal, Y.: Bovine serum albumin observed by infrared spectrometry. I. Methodology, structural investigation, and water uptake. Biopolymers **62**, 40–53 (2001). https://doi.org/10.1002/1097-0282(2001)62:1<40::AID-BIP60>3.0.CO;2-C

30. Thielges, M.C., Zimmermann, J., Dawson, P.E., Romesberg, F.E.: The determinants of stability and folding in evolutionarily diverged cytochromes *c*. J. Mol. Biol. **388**, 159–167 (2009). https://doi.org/10.1016/j.jmb.2009.02.059

31. Heimburg, T., Marsh, D.: Investigation of secondary and tertiary structural changes of cytochrome c in complexes with anionic lipids using amide hydrogen exchange measurements: an FTIR study. Biophys. J. **65**, 2408–2417 (1993). https://doi.org/10.1016/S0006-3495(93)81299-2

32. Ye, M., Zhang, Q.-L., Li, H., Weng, Y.-X., Wang, W.-C., Qiu, X.-G.: Infrared spectroscopic discrimination between the loop and α-helices and determination of the loop diffusion kinetics by temperature-jump time-resolved infrared spectroscopy for cytochrome *c*. Biophys. J. **93**, 2756–2766 (2007). https://doi.org/10.1529/biophysj.107.106799

33. von Hippel, A.R.: The dielectric relaxation spectra of water, ice, and aqueous solutions, and their interpretation. I. Critical survey of the status-quo for water. IEEE Trans. Electr. Insul. **23**, 801–816 (1988). https://doi.org/10.1109/14.8745

34. Eisenberg, D., Kautzmann, W.: The Structure and Properties of Water. Oxford University Press, New York (1969)

35. Yamamoto, N., Ohta, K., Tamura, A., Tominaga, K.: Broadband dielectric spectroscopy on lysozyme in the sub-gigahertz to terahertz frequency regions: effects of hydration and thermal excitation. J. Phys. Chem. B **120**, 4743–4755 (2016). https://doi.org/10.1021/acs.jpcb.6b01491

36. Urabe, H., Sugawara, Y., Ataka, M., Rupprecht, A.: Low-frequency Raman spectra of lysozyme crystals and oriented DNA films: dynamics of crystal water. Biophys. J. **74**, 1533–1540 (1998). https://doi.org/10.1016/S0006-3495(98)77865-8

37. Nakanishi, M., Sokolov, A.P.: Protein dynamics in a broad frequency range: dielectric spectroscopy studies. J. Non-Cryst. Solids **407**, 478–485 (2015). https://doi.org/10.1016/j.jnoncrysol.2014.08.057

38. Khodadadi, S., Pawlus, S., Sokolov, A.P.: Influence of hydration on protein dynamics: combining dielectric and neutron scattering spectroscopy data. J. Phys. Chem. B **112**, 14273–14280 (2008). https://doi.org/10.1021/jp8059807

39. Bertie, J.E., Labbé, H.J., Whalley, E.: Absorptivity of ice I in the range 4000–30 cm^{-1}. J. Chem. Phys. **50**, 4501–4520 (1969). https://doi.org/10.1063/1.1670922

40. Buckingham, A.D.: The hydrogen bond, and the structure and properties of H_2O and $(H_2O)2$. J. Mol. Struct. **250**, 111–118 (1991). https://doi.org/10.1016/0022-2860(91)85023-V

41. Bagchi, B.: Water dynamics in the hydration layer around proteins and micelles. (2005). https://doi.org/10.1021/CR020661+

42. Qvist, J., Persson, E., Mattea, C., Halle, B.: Time scales of water dynamics at biological interfaces: peptides, proteins and cells. Faraday Discuss. **141**, 131–144. **discussion 175-207** (2009)

43. Sasisanker, P., Weingärtner, H.: Hydration dynamics of water near an amphiphilic model peptide at low hydration levels: a dielectric relaxation study. ChemPhysChem **9**, 2802–2808 (2008). https://doi.org/10.1002/cphc.200800508

44. Khodadadi, S., Sokolov, A.P.: Protein dynamics: from rattling in a cage to structural relaxation. Soft Matter **11**, 4984–4998 (2015). https://doi.org/10.1039/C5SM00636H

45. He, Y., Chen, J.-Y., Knab, J.R., Zheng, W., Markelz, A.G.: Evidence of protein collective motions on the picosecond timescale. Biophys. J. **100**, 1058–1065 (2011). https://doi.org/10.1016/j.bpj.2010.12.3731

46. Markelz, A.G., Knab, J.R., Chen, J.Y., He, Y.: Protein dynamical transition in terahertz dielectric response. Chem. Phys. Lett. **442**, 413–417 (2007). https://doi.org/10.1016/j.cplett.2007.05.080

47. Chen, J.-Y., Knab, J.R., Cerne, J., Markelz, A.G.: Large oxidation dependence observed in terahertz dielectric response for cytochrome c. Phys. Rev. E **72**, 40901 (2005). https://doi.org/10.1103/PhysRevE.72.040901

48. Yamamoto, K., Tominaga, K., Sasakawa, H., Tamura, A., Murakami, H., Ohtake, H., Sarukura, N.: Far-infrared absorption measurements of polypeptides and cytochrome c by THz radiation. Bull. Chem. Soc. Jpn. **75**, 1083–1092 (2002). https://doi.org/10.1246/bcsj.75.1083

49. Markelz, A., Roitberg, A., Heilweil, E.: Pulsed terahertz spectroscopy of DNA, bovine serum albumin and collagen between 0.1 and 2.0 THz. Chem. Phys. Lett. **320**, 42–48 (2000). https://doi.org/10.1016/S0009-2614(00)00227-X

50. Mernea, M., Calborean, O., Grigore, O., Dascalu, T., Mihailescu, D.F.: Validation of protein structural models using THz spectroscopy: a promising approach to solve three-dimensional structures. Opt. Quant. Electron. **46**, 505–514 (2014). https://doi.org/10.1007/s11082-013-9872-0

51. Acbas, G., Niessen, K.A., Snell, E.H., Markelz, A.G.: Optical measurements of long-range protein vibrations. Nat. Commun. **6**, 3076 (2014). https://doi.org/10.1038/ncomms4076

52. Balu, R., Zhang, H., Zukowski, E., Chen, J.-Y., Markelz, A.G., Gregurick, S.K.: Terahertz spectroscopy of bacteriorhodopsin and rhodopsin: similarities and differences. Biophys. J. **94**, 3217–3226 (2008). https://doi.org/10.1529/biophysj.107.105163

53. Xu, J., Plaxco, K.W., Allen, S.J.: Probing the collective vibrational dynamics of a protein in liquid water by terahertz absorption spectroscopy. Protein Sci. **15**, 1175–1181 (2006). https://doi.org/10.1110/ps.062073506

54. Markelz, A., Whitmire, S., Hillebrecht, J., Birge, R.: THz time domain spectroscopy of biomolecular conformational modes. Phys. Med. Biol. **47**, 3797–3805 (2002). https://doi.org/10.1088/0031-9155/47/21/318

55. Balog, E., Becker, T., Oettl, M., Lechner, R., Daniel, R., Finney, J., Smith, J.C.: Direct determination of vibrational density of states change on ligand binding to a protein. Phys. Rev. Lett. **93**, 28103 (2004). https://doi.org/10.1103/PhysRevLett.93.028103

56. MacKerell, A.D., Bashford, D., Bellott, M., Dunbrack, R.L., Evanseck, J.D., Field, M.J., Fischer, S., Gao, J., Guo, H., Ha, S., Joseph-McCarthy, D., Kuchnir, L., Kuczera, K., Lau, F.T., Mattos, C., Michnick, S., Ngo, T., Nguyen, D.T., Prodhom, B., Reiher, W.E., Roux, B., Schlenkrich, M., Smith, J.C., Stote, R., Straub, J., Watanabe, M., Wiórkiewicz-Kuczera, J., Yin, D., Karplus, M.: All-atom empirical potential for molecular modeling and dynamics studies of proteins. J. Phys. Chem. B **102**, 3586–3616 (1998). https://doi.org/10.1021/jp973084f

57. Smith, J.C.: Protein dynamics: comparison of simulations with inelastic neutron scattering experiments. Q. Rev. Biophys. **24**, 227–291 (1991)

58. Hayward, S., Kitao, A., Hirata, F., Gō, N.: Effect of solvent on collective motions in globular protein. J. Mol. Biol. **234**, 1207–1217 (1993). https://doi.org/10.1006/jmbi.1993.1671

59. Go, N., Noguti, T., Nishikawa, T.: Dynamics of a small globular protein in terms of low-frequency vibrational modes. Proc. Natl. Acad. Sci. U. S. A. **80**, 3696–3700 (1983)
60. Rasmussen, B.F., Stock, A.M., Ringe, D., Petsko, G.A.: Crystalline ribonuclease a loses function below the dynamical transition at 220 K. Nature **357**, 423–424 (1992). https://doi.org/10.1038/357423a0
61. Sokolov, A.P., Roh, J.H., Mamontov, E., García Sakai, V.: Role of hydration water in dynamics of biological macromolecules. Chem. Phys. **345**, 212–218 (2008). https://doi.org/10.1016/j.chemphys.2007.07.013
62. He, Y., Ku, P., Knab, J., Chen, J., Markelz, A.: Protein dynamical transition does not require protein structure. Phys. Rev. Lett. **101**, 178103 (2008). https://doi.org/10.1103/PhysRevLett.101.178103